



HAL
open science

Discovery of a New Local Group Dwarf Galaxy Candidate in UNIONS: Boötes V

Simon E. T. Smith, Jaclyn Jensen, Joel Roediger, Federico Sestito, Christian R. Hayes, Alan W. Mcconnachie, Jean-Charles Cuillandre, Stephen Gwyn, Eugene Magnier, Ken Chambers, et al.

► **To cite this version:**

Simon E. T. Smith, Jaclyn Jensen, Joel Roediger, Federico Sestito, Christian R. Hayes, et al.. Discovery of a New Local Group Dwarf Galaxy Candidate in UNIONS: Boötes V. *The Astronomical Journal*, 2023, 166, 10.3847/1538-3881/acdd77 . insu-04178473

HAL Id: insu-04178473

<https://insu.hal.science/insu-04178473>

Submitted on 9 Nov 2023

HAL is a multi-disciplinary open access archive for the deposit and dissemination of scientific research documents, whether they are published or not. The documents may come from teaching and research institutions in France or abroad, or from public or private research centers.

L'archive ouverte pluridisciplinaire **HAL**, est destinée au dépôt et à la diffusion de documents scientifiques de niveau recherche, publiés ou non, émanant des établissements d'enseignement et de recherche français ou étrangers, des laboratoires publics ou privés.



Distributed under a Creative Commons Attribution 4.0 International License



Discovery of a New Local Group Dwarf Galaxy Candidate in UNIONS: Boötes V

Simon E. T. Smith¹, Jaclyn Jensen¹, Joel Roediger², Federico Sestito¹, Christian R. Hayes², Alan W. McConnachie^{1,2}, Jean-Charles Cuillandre³, Stephen Gwyn², Eugene Magnier⁴, Ken Chambers⁴, Francois Hammer⁵, Mike J. Hudson^{6,7,8}, Nicolas Martin^{9,10}, Julio Navarro¹, and Douglas Scott¹¹

¹ Department of Physics and Astronomy, University of Victoria, Victoria, BC, V8P 1A1, Canada

² NRC Herzberg Astronomy and Astrophysics, 5071 West Saanich Road, Victoria, BC, V9E 2E7, Canada

³ AIM, CEA, CNRS, Université Paris-Saclay, Université Paris, F-91191 Gif-sur-Yvette, France

⁴ Institute for Astronomy, University of Hawaii, 2680 Woodlawn Drive, Honolulu HI 96822, USA

⁵ GEPI, Observatoire de Paris, Université PSL, CNRS, Place Jules Janssen F-92195, Meudon, France

⁶ Department of Physics and Astronomy, University of Waterloo, 200 University Avenue W, Waterloo, ON N2L 3G1, Canada

⁷ Waterloo Centre for Astrophysics, University of Waterloo, 200 University Avenue W, Waterloo, ON N2L 3G1, Canada

⁸ Perimeter Institute for Theoretical Physics, 31 Caroline Street North, Waterloo, ON N2L 2Y5, Canada

⁹ Université de Strasbourg, CNRS, Observatoire astronomique de Strasbourg, UMR 7550, F-67000 Strasbourg, France

¹⁰ Max-Planck-Institut für Astronomie, Königstuhl 17, D-69117, Heidelberg, Germany

¹¹ Department of Physics & Astronomy, University of British Columbia, Vancouver, BC, V6T 1Z1, Canada

Received 2022 September 16; revised 2022 November 3; accepted 2022 November 3; published 2023 July 28

Abstract

We present the discovery of Boötes V, a new ultra-faint dwarf galaxy (UFD) candidate. This satellite is detected as a resolved overdensity of stars during an ongoing search for new Local Group dwarf galaxy candidates in the UNIONS photometric data set. It has a physical half-light radius of $26.9_{-5.4}^{+7.5}$ pc, a V-band magnitude of -4.5 ± 0.4 mag, and resides at a heliocentric distance of approximately 100 kpc. We use Gaia DR3 astrometry to identify member stars, characterize the systemic proper motion, and confirm the reality of this faint stellar system. The brightest star in this system was followed up using Gemini GMOS-N long-slit spectroscopy and is measured to have a metallicity of $[\text{Fe}/\text{H}] = -2.85 \pm 0.10$ dex and a heliocentric radial velocity of $v_r = 5.1 \pm 13.4$ km s⁻¹. Boötes V is larger (in terms of scale radius), more distant, and more metal-poor than the vast majority of globular clusters. It is likely that Boötes V is an UFD, though future spectroscopic studies will be necessary to definitively classify this object.

Unified Astronomy Thesaurus concepts: Dwarf galaxies (416); Local Group (929); Broad band photometry (184); Milky Way stellar halo (1060)

1. Introduction

The discovery and study of dwarf galaxies in the Local Group has prospered due to the great advances in wide-field imaging surveys over the last two decades (e.g., Willman et al. 2005a, 2005b; Belokurov et al. 2006, 2007, 2008; Koposov et al. 2015a; Laevens et al. 2015a, 2015b; Torrealba et al. 2016, 2018, 2019; Mau et al. 2020; Cerny et al. 2021a, 2021b, Cerny et al. 2023b; Sand et al. 2022). The Sloan Digital Sky Survey (SDSS; York et al. 2000; Abazajian et al. 2009) led the early charge, with the Pan-STARRS consortium (Chambers et al. 2016), the Dark Energy Survey (DES; Abbott et al. 2018), and the DECam Local Volume Exploration Survey (DELVE; Drlica-Wagner et al. 2021) contributing mightily to the discovery of Milky Way satellites, while the Pan-Andromeda Archaeological Survey (McConnachie et al. 2009) has been prolific in finding dwarf galaxies around M31 (e.g., McConnachie et al. 2008; Richardson et al. 2011; Martin et al. 2013). The dwarf galaxy population around M31 has also been bolstered by more recent work with the DESI Legacy Imaging Survey (Dey et al. 2019; Collins et al. 2022; Martínez-Delgado et al. 2022).

Dwarf galaxies play several key roles in testing and developing new models for answering some of the most fundamental questions in astronomy. Dwarf galaxies fainter

than around $M_V = -7.7$ have been dubbed “ultra-faint dwarf galaxies” (UFDs; e.g., see review by Simon 2019). They appear to be the smallest, least-massive, and most metal-poor galaxies yet observed, and so represent the extreme end of the galaxy luminosity function. They appear to reside in the shallowest gravitational potential wells that have been able to retain gas and stars throughout cosmic time (e.g., Bovill & Ricotti 2009; Simon 2019), and their existence tests current theories of galaxy formation, particularly the interplay between stellar feedback and gas retention (Bullock & Boylan-Kolchin 2017), the evolution of faint galaxies in the Milky Way environment (e.g., Wheeler et al. 2015), and the quenching effects of reionization (e.g., Bullock et al. 2000). Critically, UFDs are powerful probes of theories of structure evolution, as they provide parsec-scale tests of dark matter models that were initially developed to explain the largest-scale observations of the universe (Lovell et al. 2012; Bullock & Boylan-Kolchin 2017). Discoveries of new Local Group dwarf galaxies continue to provide both unique individual examples and an ever-growing statistical sample of faint systems that are testing these aforementioned fundamental theories of structure and galactic evolution.

In this paper, we detail the discovery and characterization of a new UFD candidate, which we call Boötes V. In Section 2 we summarize the data set in which it was detected and the search algorithm that was used. In Section 3, we characterize the structural parameters of the dwarf galaxy candidate, as well as its distance and luminosity. In Section 4, we identify member



Original content from this work may be used under the terms of the [Creative Commons Attribution 4.0 licence](https://creativecommons.org/licenses/by/4.0/). Any further distribution of this work must maintain attribution to the author(s) and the title of the work, journal citation and DOI.

stars observed with Gaia, measure the proper motion of the system, and present first estimates of its metallicity and dynamics. Finally, in Section 5, we discuss the classification of Boötes V and summarize our results. Additionally, we draw the attention of the reader to the work of Cerny et al. (2023a), which presents an independent discovery of this new satellite in the DELVE data set (Drlica-Wagner et al. 2021, 2022).

2. Data and Detection

2.1. UNIONS

Boötes V was identified as an overdensity of resolved stars in the Ultraviolet Near-Infrared Optical Northern Survey (UNIONS). UNIONS is a consortium of northern wide-field imaging surveys, and consists of the Canada-France Imaging Survey (CFIS) collaboration that uses the Canada–France–Hawaii Telescope (CFHT), team members from Pan-STARRS, and the Wide Imaging with Subaru HyperSuprime-Cam of the Euclid Sky (WISHES). Each group is currently collecting imaging at their respective telescopes: CFHT/CFIS is targeting deep u - and r -band photometry, Pan-STARRS is obtaining deep i and moderate/deep z bands, and Subaru/WISHES is acquiring the deep z band. These independent efforts are directed, in part, to securing optical imaging to complement the Euclid space mission, although UNIONS is a separate consortium aimed at maximizing the science return of these large and deep ground-based surveys of the northern skies. When completed, the combined $ugriz$ survey will cover approximately 5000 deg^2 at declinations of $\delta > 30^\circ$ and Galactic latitudes of $|b| > 30^\circ$ (the northern sky, excluding the Milky Way disk) and will be approximately as deep as 1 yr of the Legacy Survey of Space and Time at the Vera C. Rubin Observatory.

Our work uses the CFIS- r and Pan-STARRS- i combined data set. For CFIS- r , the 5σ point-source depth is 24.9 mag with a $2''$ aperture. For Pan-STARRS- i , the final 5σ point-source depth will be 24.3 mag. However, the Pan-STARRS survey strategy of mapping the entire sky repeatedly means that the i band is currently, on average, at about 75% of the final depth, although there is significant variation across the survey region. The area in common between both bands at this stage amounts to $\sim 3500 \text{ deg}^2$ total across both the North and South Galactic Caps. These catalogs were crossed matched using a $0''.5$ matching tolerance (although typically the sources match to better than $0''.13$).

Star–galaxy separation was performed using morphological criteria in CFIS- r , which has a median image quality of better than $0''.7$. We correct for the Galactic foreground extinction using the extinction values, $E(B - V)$, from Schlegel et al. (1998) assuming the conversion factors given by Schlafly & Finkbeiner (2011) for a reddening parameter of $R_V = 3.1$. For the CFIS- r , we adopt the conversion factor for the DES r band: the FWHM of the DES- r (Flaugher et al. 2015) and CFIS- r are identical, and the DES r band is shifted redward with respect to the CFIS filter by only 2 nm.

2.2. GMOS-N Spectroscopy

We received Directors Discretionary Time at Gemini North to use the Gemini Multi-Object Spectrograph (GMOS-N) to obtain the spectrum of a single star, the brightest in Boötes V, through the program GN-2022B-DD-201 (PI: S. Smith). Our

long-slit spectroscopic observations used the R831 grating and the RG610 spectroscopic blocking filter, with a $1''$ wide slit. We had a 1×2 CCD binning configuration, resulting in a $\sim 0.38 \text{ \AA}$ per-pixel spectral resolution. Our observations comprised $3 \times 900 \text{ s}$ exposures centered at 8500 \AA and $3 \times 900 \text{ s}$ exposures centered at 8600 \AA during the nights of August 7 and August 8, bringing our total exposure time to 5400 s.

The science observations were reduced and extracted using standard routines and procedures for GMOS data in the Gemini IRAF package. Bias corrections and flat-fielding were performed, along with the calibration of the wavelength solution using CuAr emission lamp exposures that were taken alongside the science observations. The three frames obtained at each central wavelength were stacked using GEMCOMBINE, and a 1D spectrum was extracted from each stack. The flux was then calibrated using a 60 s exposure of a spectrophotometric standard (G191B2B) using an identical instrument setup with the observations centered at a wavelength of 8500 \AA . The 8500 \AA -centered stack and 8600 \AA -centered stack were observed on consecutive nights, so their extracted spectra were individually corrected for Earth’s orbital motion about the Sun before they were added together, producing the final spectrum of the target star.

The exposure times, instrument setup, and wavelength range were selected with the goal of measuring a signal-to-noise ratio of ~ 50 per-pixel in the region of the Calcium II infrared triplet (CaT) absorption feature. This has been demonstrated as sufficient to measure the heliocentric radial velocity with an uncertainty of $\sim 10 \text{ km s}^{-1}$ (Piatti et al. 2018), and also sufficient to measure the CaT equivalent width (EW) with adequate precision for reaching an uncertainty of less than 0.2 dex in the metallicity estimate through the CaT EW-[Fe/H] relation of Starkenburg et al. (2010). Details of the measured properties of this spectrum can be found in Section 4.2.

2.3. Detection

Boötes V was identified as one of the most promising candidates in a new and ongoing search for dwarf galaxies in the UNIONS sky. The method of detection is based on a matched-filter approach, a tried and tested methodology that has yielded many previous dwarf galaxy discoveries (Martin et al. 2008; Bechtol et al. 2015; Drlica-Wagner et al. 2015). We start by selecting all stars that are consistent with a 12 Gyr, $[\text{Fe}/\text{H}] = -2$ dex isochrone shifted to a heliocentric distance d . The algorithm filters the sky systematically in logarithmic steps for d in the range $[10, 1000]$ kpc, and the isochrones used in this work were obtained from the PARSEC isochrone database (Bressan et al. 2012) for the CFHT and Pan-STARRS 1 (PS1) photometric systems. We adopt a broad color cut around the isochrone that is more than sufficient to account for the empirical photometric errors in both the CFIS- r and Pan-STARRS- i , the intrinsic color spread of any putative dwarf galaxy, and the unknown distance of the dwarf. Formally:

$$|(r - i)_{\text{star}} - (r - i)_{\text{iso}}| \leq \sqrt{0.1^2 + \sigma_r^2 + \sigma_i^2}, \quad (1)$$

where $(r - i)_{\text{star}}$ is the color of a given star, $(r - i)_{\text{iso}}$ is the color of the isochrone at the same magnitude as the given star, and $\sigma_{r,i}$ are the photometric uncertainties in each passband at the same magnitude as the given star. The algorithm does not consider stars fainter than CFIS- $r = 24.6$ and Pan-STARRS- $i = 24$, since

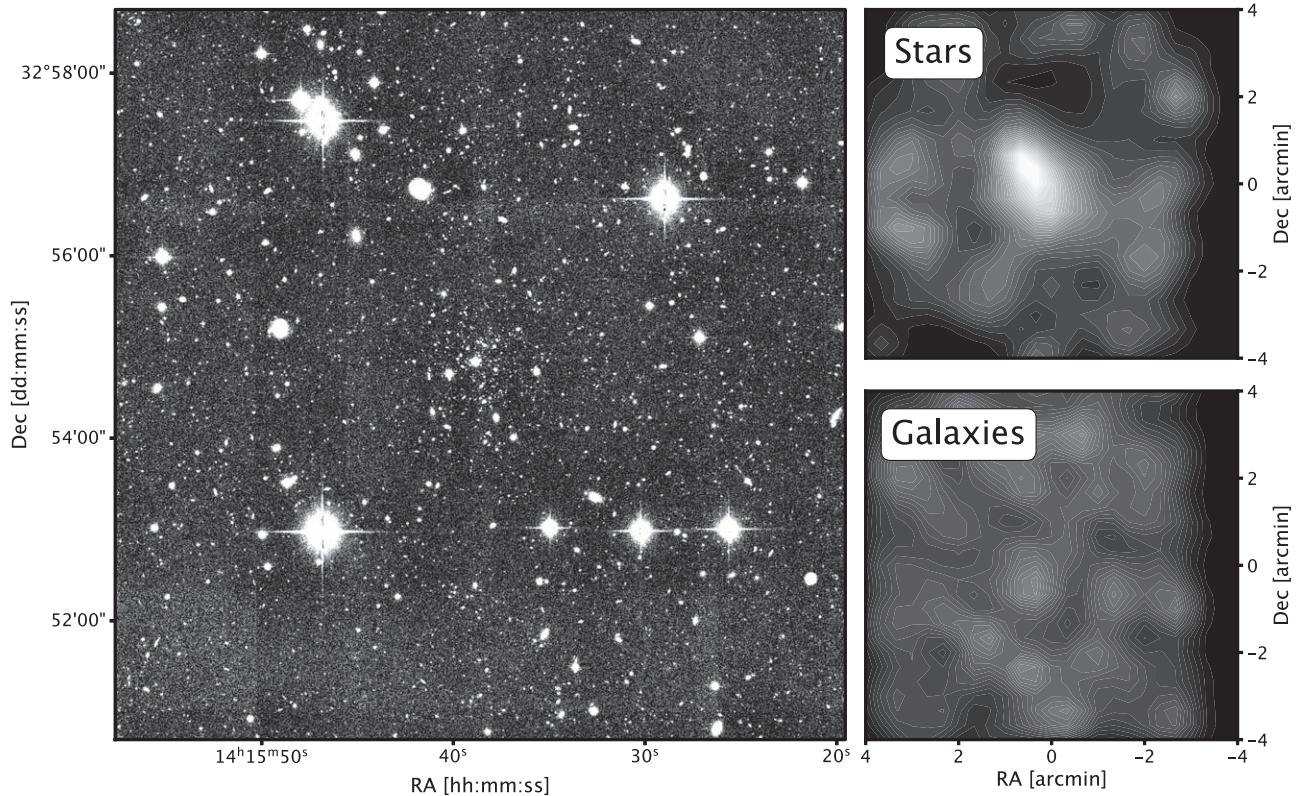


Figure 1. Left: $8' \times 8'$ cutout from CFIS- r imaging tiles. Bright sources with diffraction spikes are likely Milky Way foreground stars. The clustering of stars and light in the center of this image is Boötes V. Upper right: smoothed spatial density plot of all stellar sources on the $8' \times 8'$ tile. No stellar population filtering has been applied to the stars in this smoothed distribution. Lower right: smoothed spatial density plot of all galaxies in the $8' \times 8'$ tile, normalized with respect to the stellar density. There are many more galaxies than stars in this field of view, but there is no discernible overdensity.

below these limits completeness becomes an issue, although all detected stars are used when visually inspecting candidates. Stars meeting this color criteria are selected and projected onto the tangent plane, where they are spatially binned into 0.5×0.5 pixels. This pixel size was selected to be slightly smaller than the typical angular size of the smallest known dwarfs so that a single galaxy will appear as several pixels in the 2D stellar density map.

The next step concerns teasing out local overdensities of stars. We find the mean local stellar density for each pixel by convolving the field with a 2D top hat filter with a width of $20'$, where the large kernel was chosen to sufficiently smooth the stellar density around a putative dwarf galaxy. We find the standard deviation in the local stellar density by taking the square root of the variance of these convolved maps. By definition, this is the square of the mean local density minus the mean of the squared local density, i.e.,

$$\sigma_{\text{loc}} = \sqrt{\langle \rho_{\text{loc}}^2 \rangle - \langle \rho_{\text{loc}} \rangle^2}. \quad (2)$$

ρ_{loc} is the density of the local field, and σ_{loc} is the standard deviation in the local field.

Returning to the unsmoothed distributions, we convolve these maps with 2D Gaussian kernels of different sizes, corresponding to dwarf galaxies with different projected sizes. Specifically, we adopt kernels with an FWHM of 1.2 , 2.4 , and 4.8 . We refer to these “smoothed densities” as ρ_{sm} . Finally, for the entire UNIONS sky, we compute a 2D map of the statistical

overdensities with respect to the local stellar density as

$$s = \frac{\rho_{\text{sm}} - \rho_{\text{loc}}}{\sigma_{\text{loc}}}, \quad (3)$$

where s is the significance of the overdensity in units of σ_{loc} . This process is repeated for a range of distances, where each distance produces three maps, one for each of the smoothing kernels.

During initial tests of this method, nearly all known dwarf galaxies in the UNIONS footprint have been detected with high significance. As a reference point, Canes Venatici II is detected with high significance at several distances. At a distance of 100 kpc, with the stellar density map smoothed by a $1.2''$ kernel, Canes Venatici II (true distance of 160 kpc) has $s = 2.8$, while Boötes V has a significance value of $s = 4.9$. Boötes V is detected strongly at many distances less than 150 kpc and is one of the most prominent overdensities of match-filtered stars that has not previously been identified as a real stellar system. However, we note the work of Darragh-Ford et al. (2021), who have developed a wavelet-based algorithm to search for dwarf galaxy candidates in the Gaia data set. Boötes V was identified as a “gold standard” candidate in position–proper-motion space, though their work did not present a follow-up study.

In support of the match-filter detection, we present the CFIS- r imaging of the putative dwarf galaxy (left panel of Figure 1) wherein a central clustering of sources is seen prominently. As mentioned in Section 2.1, we separate sources in the imaging into stars and galaxies, and in the right panels of Figure 1, we

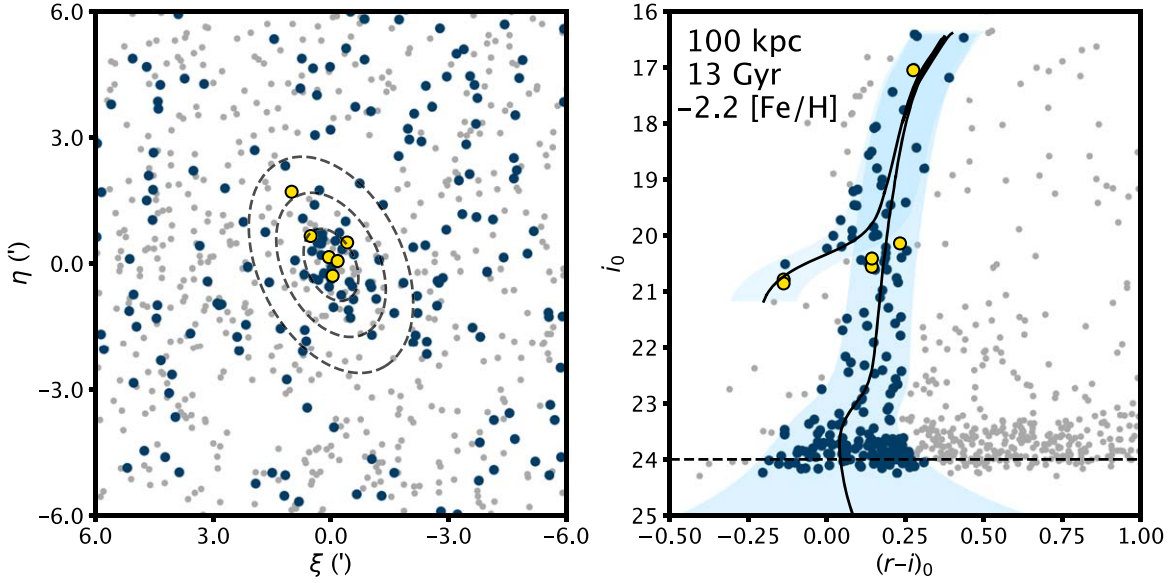


Figure 2. Left: sky positions of all stars in a $12' \times 12'$ region about Boötes V, projected onto the tangent plane centered at R.A., decl. = ($14^{\text{h}}15^{\text{m}}38^{\text{s}}.6$, $+32^{\circ}54'42''$). Dark blue sources are those that meet the isochrone selection criterion (see right panel). Yellow points are stars identified in Gaia DR3 as sources with complete astrometric information, and are selected as high-confidence (probability $> 90\%$) members by our maximum-likelihood membership selection algorithm (see Section 4.1). The concentric black ellipses indicate $1 \times$, $3 \times$, and $5 \times$ the half-light radius (r_{h}) as determined by the Markov Chain Monte Carlo (MCMC) fit (see Section 3.1). Right: CMD of extinction-corrected CFIS- r and Pan-STARRS- i for all stellar sources in a $12' \times 12'$ region about Boötes V. We overlay an old (13 Gyr), metal-poor ($[\text{Fe}/\text{H}] = -2.2$) isochrone, shifted to a distance of 100 kpc. We use a broad color selection criterion, selecting all stars with $(r-i)_0 \leq 0.1$ from the isochrone, and we add, in quadrature, the empirical photometric errors from each band. Stars consistent with this selection criterion are highlighted in dark blue.

show the surface density of both of these. Clearly, the clustering is not due to background galaxies.

We show the spatial density of the match-filter-selected stars alongside the color-magnitude diagram (CMD) of sources in the vicinity of Boötes V in Figure 2. The positions of all of these sources on the CMD suggest that many of the stars in this field of view are consistent with the same old, metal-poor stellar population given a putative distance to the system of 100 kpc.

3. Photometric and Structural Properties

3.1. Structure

Given the probable identification of a new Milky Way satellite as shown in Figure 2, we determine the most likely values of its structural parameters using a Markov Chain Monte Carlo (MCMC) approach under the assumption that the system is well described by an exponential model.

Our model and approach are based on the work in Martin et al. (2008) and Martin et al. (2016), and we used `emcee` (Foreman-Mackey et al. 2013) to sample the posterior. The radial surface density profile $\rho_{\text{dwarf}}(r)$ for a dwarf galaxy can be described with an elliptical, exponential model as a function of r . This profile is defined by the centroid of the profile (x_0, y_0) , an ellipticity ϵ (defined as $\epsilon = 1 - b/a$ where b/a is the minor-to-major-axis ratio of the model), the position angle of the major axis θ , (defined east of north), the half-light radius (which is the length of the semimajor axis r_{h}), and the number of stars N^* in the system. The model is written as

$$\rho_{\text{dwarf}}(r) = \frac{1.68^2}{2\pi r_{\text{h}}^2 (1 - \epsilon)} N^* \exp\left(\frac{-1.68r}{r_{\text{h}}}\right), \quad (4)$$

where r , the elliptical radius, is related to the projected sky coordinates (x, y) by

$$r = \left\{ \left[\frac{1}{1 - \epsilon} ((x - x_0)\cos\theta - (y - y_0)\sin\theta) \right]^2 + [((x - x_0)\sin\theta - (y - y_0)\cos\theta)^2] \right\}^{\frac{1}{2}}. \quad (5)$$

We assume that the background stellar density is constant, which is reasonable on the scale of arcminutes up to a degree or so. As such, we model the density of stars in our entire field of view as

$$\rho_{\text{model}}(r) = \rho_{\text{dwarf}}(r) + \Sigma_{\text{b}}, \quad (6)$$

where Σ_{b} is the constant background density term. This term is defined to be

$$\Sigma_{\text{b}} = \frac{n - N^*}{A}, \quad (7)$$

where n is the total number of stars in the field of view, and A is the total area, normalizing the background density with respect to the selected region.

We use all matched-filter selected sources within a circle of radius $9'$ surrounding the satellite's initial centroid, projected onto the tangent plane. We constrain the centroid to a central box with side lengths of $12'$ and restrict the half-light radius to a maximum size of $6'$. Constraints for all model parameters can be found in Table 1, and we assume flat priors between the presented bounds in all cases. The `emcee` program used 64 walkers, each going through 15,000 iterations, and the first 7500 iterations were thrown out to account for burn-in. Through this analysis, we find that Boötes V is located at an R.A. of $14^{\text{h}}15^{\text{m}}38^{\text{s}}.6$ and a decl. of $+32^{\circ}54'40''$. We present the results of the MCMC analysis as a corner plot in Figure 3, and we include the final parameter estimates alongside all other measured and derived properties of Boötes V in Table 2.

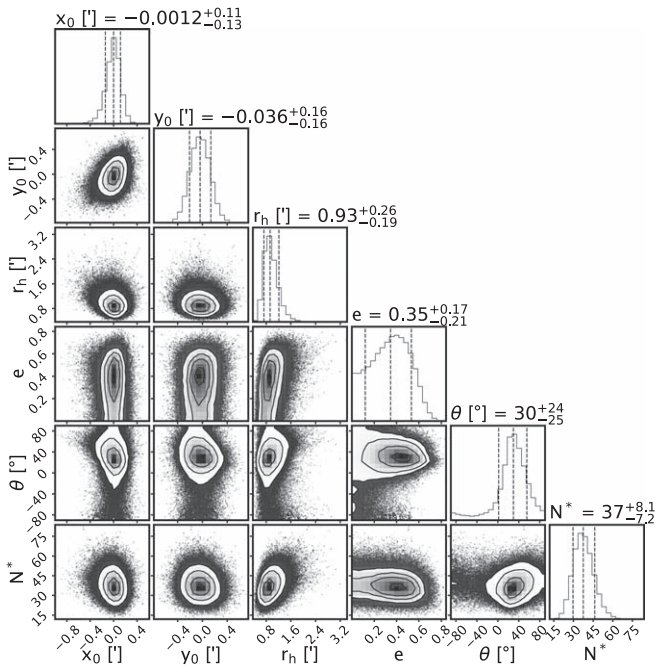


Figure 3. Two-dimensional and marginalized probability distribution functions (PDFs) from the MCMC analysis. The fit was run on all stellar sources within a $9'$ radius, circular region around the initial satellite's centroid estimate that are consistent with the isochrone selection criteria. This corresponds to all of the stars that are highlighted in blue in Figure 2. The quantities x_0 , y_0 , and r_h are the projected R.A. centroid offset, projected decl. centroid offset, and half-light radius, respectively. All three are presented in arcminutes. Ellipticity is denoted as $\epsilon = 1 - b/a$, where b/a is the minor-to-major axis ratio, while θ is the position angle (denoted east from north in degrees), and N^* is the estimated number of member stars. In each marginalized PDF, dashed lines should be interpreted as the 16th, 50th, and 84th quantiles, from left to right.

3.2. Distance Determination

Boötes V was initially identified as an overdensity of stars at around 100 kpc. Given this initial distance estimate, comparisons to isochrones suggested that there may be a potential member star near the tip of the red giant branch (RGB), as well as three possible member stars consistent with being blue horizontal branch (BHB) stars. These are shown as a red triangle and blue squares, respectively, in Figure 4. Note that the two brightest BHB candidates occupy an almost identical position in this figure.

Under the assumption that the bright star is indeed an RGB star, we can estimate the distance to Boötes V by assuming that this star is at the tip of the RGB (TRGB). This is the upper bound on the distance estimate, as the lone, bright star may not truly be at the very tip, and there are no other similarly bright stars in the system with which to compare.

The TRGB in the I band has been shown to act as a standard candle and can therefore be used for distance estimation (Lee et al. 1993; Salaris & Cassisi 1997). As we are working in the Pan-STARRS- i band, we estimate the i -band TRGB absolute magnitude empirically using PARSEC isochrones (Bressan et al. 2012). Using isochrones of 12 and 13 Gyr, and considering $[\text{Fe}/\text{H}]$ in the range $[-2.2, -1]$ dex in intervals of 0.1 dex, we find the mean i -band TRGB to be 3.51 ± 0.04 mag. We also take into account the statistical uncertainty (0.05 mag) and the systematic uncertainty (0.08 mag) from the globular cluster calibration of the I -band TRGB by Freedman et al. (2020), giving $M_i^{\text{TRGB}} =$

Table 1
Flat Priors for Each Parameter in the MCMC Analysis

Parameter	Prior
x_0	$-6' < \Delta x_0 < +6'$
y_0	$-6' < \Delta y_0 < +6'$
r_h	$0 < r_h < 6'$
ϵ	$0 < \epsilon < 1$
θ	$-90^\circ < \theta < +90^\circ$
N^*	$0 < N^* < 100$

3.51 ± 0.10 mag. The corrected i -band luminosity of the RGB star in question is $i_0 = 17.05 \pm 0.02$ mag, yielding a distance modulus of $(m - M)_i = 20.57 \pm 0.10$ mag. The upper bound on the distance to Boötes V is therefore $d_{\text{upper}} = 130 \pm 6$ kpc.

For determining the distance to the potential BHB stars, we follow the calibration given by Deason et al. (2011) for the absolute g -band magnitude of BHB stars using SDSS g - and r -band magnitudes:

$$M_g = 0.434 - 0.169(g_0 - r_0) + 2.319(g_0 - r_0)^2 + 20.449(g_0 - r_0)^3 + 94.517(g_0 - r_0)^4. \quad (8)$$

All three potential BHB stars are in SDSS DR17, and their extinction-corrected SDSS g - and r -magnitudes are presented in Table 3. The faintest BHB star has $(g_0 - r_0) = -0.34$, which falls outside the color range for which the above equation is valid ($-0.25 < (g_0 - r_0) < 0$; see Deason et al. 2011 for details), so we cannot use it for a distance estimate. Table 3 presents derived absolute g -magnitudes and distances for the two bright BHBs. They have heliocentric distances of 97.4 ± 2.8 and 97.4 ± 3.2 kpc, where the uncertainties are only those obtained by propagating the uncertainties in magnitudes.

A third estimate of the distance may be measured by estimating the distance an isochrone should be shifted to in order to best match the CMD. As such, we determined the best-match isochrone through visual inspection by adopting a 13 Gyr stellar population, and considering $[\text{Fe}/\text{H}]$ in the range $[-2.2, -1.9]$ dex in intervals of 0.1 dex, and distance shifts in the range $[80, 175]$ kpc in intervals of 5 kpc. We found that an isochrone of $[\text{Fe}/\text{H}] = -2.2$ dex, the most metal-poor isochrone available in our set, shifted to a distance of 100 ± 20 kpc describes the data reasonably well. Figure 4 shows the CMD of all stars within 3 elliptical r_h , with the isochrone overlaid at distances of 80, 100, and 120 kpc, to demonstrate the range we estimate as reasonable: much closer or much more distant, and the isochrone (both the hydrogen and helium burning branches) does not align well with the bulk of the stars, especially, but not only, with the BHB and RGB candidates discussed earlier.

While each of these methods of estimating the distance to this satellite is imprecise, they all point to a distance of approximately 100 kpc. Consequently, for the remainder of our analysis, we adopt a distance to the satellite of 100 ± 20 kpc. This estimate from the by-eye isochrone analysis is fully consistent with estimates from both BHB stars and the upper limit provided by the candidate RGB star.

We searched the PS1 RR Lyrae (Sesar et al. 2017) and Gaia variability (Gaia Collaboration 2022) catalogs, but could not find evidence that any RR Lyrae stars have been detected, so

Table 2
Measured and Derived Properties for Boötes V

Property	Description	Value
α_{J2000}	R.A.	$14^{\text{h}}15^{\text{m}}38.6_{-0.6}^{+0.5\text{s}}$
δ_{J2000}	decl.	$+32^{\circ}54'40_{-10}^{+9.2''}$
$r_{\text{h, ang}}$	Angular half-light radius	$0.93_{-0.19}^{+0.26'}$
$r_{\text{h, phys}}$	Physical half-light radius	$26.9_{-5.4}^{+7.5}$ pc
ϵ	Ellipticity	$0.35_{-0.21}^{+0.17}$
θ	Position angle	$30_{-25}^{+24^{\circ}}$
N^*	Number of stars	$37_{-7.2}^{+8.1}$
d	Heliocentric distance	100 ± 20 kpc
$E(B - V)$	Average $E(B - V)$, $2' \times 2'$ box	0.013
M_V	Absolute V -band magnitude	-4.5 ± 0.4 mag
M_r	Absolute r -band magnitude	-4.9 ± 0.4 mag
M_i	Absolute i -band magnitude	-5.2 ± 0.4 mag
μ_{eff}	effective surface brightness	25.7 ± 0.7 mag arcsec $^{-2}$
$\mu_{\alpha} \cos \delta$	Proper motion in R.A.	-0.23 ± 0.04 (stat) ± 0.033 (sys) mas year $^{-1}$
μ_{δ}	Proper motion in decl.	-0.28 ± 0.07 (stat) ± 0.033 (sys) mas year $^{-1}$
v_r	Radial velocity [GMOS-N]	$+5.1 \pm 13.4$ km s $^{-1}$
[Fe/H]	Metallicity [GMOS-N]	-2.85 ± 0.10 dex

Note. Statistical errors on the proper-motion measurements come from the maximum-likelihood analysis described in Section 4.1. Systemic errors were investigated by Lindegren et al. (2021).

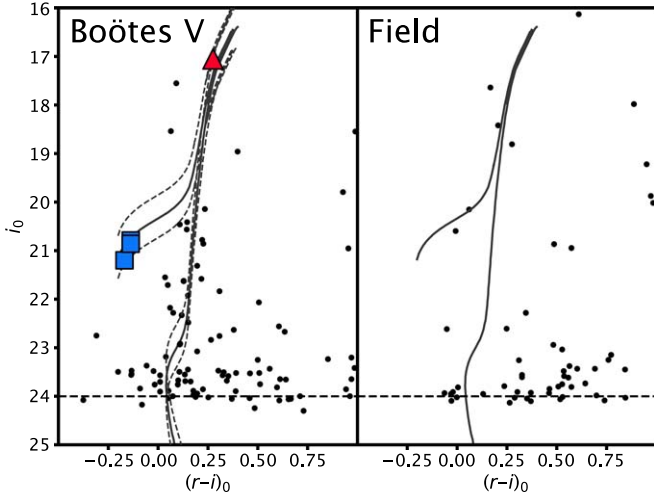


Figure 4. Left: CMD of all stars within 3 elliptical r_{h} of the satellite’s centroid; 92 stars meet this spatial criterion. A 13 Gyr, $[\text{Fe}/\text{H}] = -2.2$ isochrone shifted to 100 kpc is overlaid as a solid line. Isochrones shifted to 80 and 120 kpc, the lower and upper distance bounds as determined in Section 3.2, are shown as dashed lines. A possible TRGB star (red triangle) and three possible BHB stars (blue squares), which were used for distance estimates, are shown as well. Note that the two brightest BHB stars are nearly directly atop each other on the CMD. Right: CMD of stars within an equivalent area offset by $12'$ to the south of the satellite’s centroid, with the same isochrone overlaid; 48 stars meet this spatial criteria.

we unfortunately cannot use the properties of these variable stars to constrain the distance to Boötes V.

3.3. Luminosity

To estimate the luminosity of Boötes V, we use an approach that is based on the work of Martin et al. (2016), which aims to create a suite of synthetic stellar populations that represent the full stellar content of the dwarf galaxy. The construction of

each individual synthetic stellar population is performed as follows.

We assume that the stellar population in question is well represented by a 13 Gyr, $[\text{Fe}/\text{H}] = -2.2$ PARSEC isochrone (Bressan et al. 2012), with a standard Kroupa initial mass function (Kroupa 2001), which has been corrected for Galactic foreground extinction (same as the description in Section 2.1). We then draw a random distance from a normal distribution centered at 100 kpc, with a standard deviation of 20 kpc, and shift the isochrone to that distance. We then construct an i -band luminosity function (ignoring the horizontal branch) down to $0.1 M_{\odot}$, and normalize it so that it behaves as a probability distribution function (PDF).

Crucially, these mock stellar populations are characterized by the number of stars above the magnitude limit of our survey, emulating the actual stellar population that was observed. We reran the MCMC analysis using only stars consistent with the main sequence and RGB that have Pan-STARRS- $i < 24$, and we found that Boötes V is estimated to have $34_{-6.5}^{+7.3}$ stars that fit these criteria. So, we also sample a normal distribution centered at 34, with a standard deviation of 6.9 (average of empirical 16th and 84th quantiles), and set this value to be N , the target number of stars in the mock stellar population brighter than the limiting magnitude of 24 mag in Pan-STARRS- i . Randomly drawing values for both the distance and the number of stars above the magnitude limits for each realization of the stellar population allows for the propagation of parameter estimate uncertainties into the final derived magnitude of the system.

Finally, to create the synthetic stellar population, we sample the PDF using the acceptance-rejection method, recording the r -band, i -band, and V -band magnitudes of each accepted star, and flagging each star that has $m_i < 24$ mag. When we accrue N flagged stars (where N is the target number of stars in that realization of Boötes V), we stop sampling. Finally, we shift apparent magnitudes to absolute magnitudes (using the distance corresponding to that specific realization of the stellar

Table 3
Identifier, Magnitudes, and Distance Information for Three Potential BHB Stars

Identifier	g_0 (mag)	r_0 (mag)	M_g (mag)	d_{BHB} (kpc)
SDSS J141543.35+325624.0	20.42 ± 0.021	20.56 ± 0.031	0.48 ± 0.058	97.4 ± 2.8
SDSS J141537.78+325445.0	20.43 ± 0.022	20.57 ± 0.032	0.48 ± 0.069	97.4 ± 3.2
SDSS J141538.35+325501.0	20.72 ± 0.026	21.05 ± 0.046

population), convert to fluxes, sum them, and convert to the total absolute magnitude.

We generate 1000 instances of the stellar population and find the systemic magnitude of Boötes V to be $M_V = -4.5 \pm 0.4$ mag. When converted into total luminosity, we get $5.4^{+2.2}_{-1.6} \times 10^3 L_\odot$. We calculate the effective surface brightness by dividing half the total flux by the area enclosed by one elliptical half-light radius and converting to $\text{mag arcsecond}^{-2}$. We calculate it to be $25.7 \pm 0.7 \text{ mag arcsecond}^{-2}$ with all errors from the magnitude, half-light radius, and ellipticity propagated through. These values, including the absolute magnitudes in the r and i bands, are included in Table 2.

4. Dynamics and Metallicity

4.1. Proper Motion, Membership Using Gaia

The third data release from Gaia (Gaia Collaboration et al. 2016, 2021) has a limiting magnitude of about $G = 21$ mag. The majority of stars we selected as members of this system based on UNIONS photometry using our matched-filter method are fainter than the Gaia limits, but several of the brighter stars are successfully detected by Gaia, allowing for the use of Gaia’s powerful astrometry (Lindegren et al. 2021) in characterizing this system, as well as providing clear confirmation of its reality.

We follow the methodology developed by McConnachie & Venn (2020a) to estimate the systemic proper motion of the system and to clearly identify member stars. The reader is referred to this paper for details. Briefly, the algorithm estimates the most likely proper motion for a putative satellite under the assumption that a field of stars consists of only a Milky Way satellite and Milky Way foreground, by considering the CMD distribution of stars, the spatial distribution of stars, and the proper-motion distribution of stars. The foreground/background density is assumed constant in the region of the putative satellite, and the CMD and proper-motion distributions of the foreground/background are derived empirically. The CMD distribution of the putative satellite assumes an old, metal-poor system at some distance, and the spatial distribution of the putative satellite assumes a 2D exponential profile described by a centroid, ellipticity, position angle, and half-light radius. As such, the distance and structural parameter estimates derived earlier (and their uncertainties) are used in this analysis. The CMD distribution is modeled as an old (13 Gyr), metal-poor ($[\text{Fe}/\text{H}] = -2.2$) isochrone in the Gaia passbands (Riello et al. 2021). Additionally, we incorporated extra constraints for robustly selecting horizontal branch stars (see J. Jensen et al. 2023, in preparation, for further details). This method assumes that the proper motions of all stars within the putative satellite share the same intrinsic proper motion, with any variance coming directly from measurement uncertainties, so that the proper-motion PDF is modeled as a bivariate Gaussian function.

For Boötes V, we follow McConnachie & Venn (2020b), and select well-measured sources in a circular region with a radius of 2° around the previously determined centroid. We identify six high-confidence members (membership probability $> 90\%$) within 3 elliptical r_h and display these stars in Figure 5. This figure shows the spatial positions, G_0 versus $(B_p - R_p)_0$ CMD, and proper motions of the six members compared to the field (gray points). We find the systemic proper motion of Boötes V to be $(\mu_\alpha \cos \delta, \mu_\delta) = (-0.23 \pm 0.04$ (stat) $+ 0.033$ (sys), -0.28 ± 0.07 (stat) $+ 0.033$ (sys)) mas year^{-1} . We note that such a tight clustering in all of these spaces, especially proper-motion space, provides a robust confirmation that this is a real physical system. Systematic errors are taken from Lindegren et al. (2021).

Encouragingly, all of these high-confidence members are also found in the original matched-filter selection that identified the stellar overdensity in UNIONS (Section 2.3). Of these six likely member stars, two are the brightest stars identified as potential BHB stars in Section 3.2. The third BHB star, which was not used for a distance estimate, does not have well-measured astrometric parameters, and so its membership cannot be classified by this method. Another of the six likely member stars is the bright RGB candidate discussed earlier. The Gaia member stars are cross-matched to the UNIONS data set and are plotted as yellow markers in Figure 2. We note that in Figure 5, several of the faintest stars appear to be HB stars that lie below the isochrone track. While this might suggest we are underestimating the distance, shifting the isochrone to larger distances only produces a reasonable fit to the data up to about 120 kpc, which is within the uncertainty we adopt when only using UNIONS data. A deeper CMD than obtained with Gaia or UNIONS is necessary to allow for a more robust distance measurement.

4.2. Spectroscopic Follow-up Analysis

In Section 3.2 we assumed that the brightest star consistent with the isochrone was a red giant star near the TRGB. Our membership analysis has also identified this star as a highly likely member (probability $> 99.9\%$). Fortunately, this star was observed as part of the Large Sky Area Multi-Object Fiber Spectroscopic Telescope (LAMOST), and has low-resolution spectroscopy available as part of its Data Release 5 (DR5). Its LAMOST stellar identifier is LAMOST HD141746N33 1518M01. LAMOST DR5 (Xiang et al. 2019) provides an estimation for both the metallicity and heliocentric radial velocity of this RGB star, with $[\text{Fe}/\text{H}] = -2.25 \pm 0.60$ dex $v_r = -5.5 \pm 22.7 \text{ km s}^{-1}$. However, the uncertainties on both measurements are rather large, which prompted us to obtain our own low-resolution spectrum of this RGB star using GMOS-N as described in Section 2.2. The analysis of the reduced spectrum is now presented.

We infer the metallicity of the star adopting the method from Starkenburg et al. (2010). Their method needs as input the EW of the second and third components of the Ca II Triplet

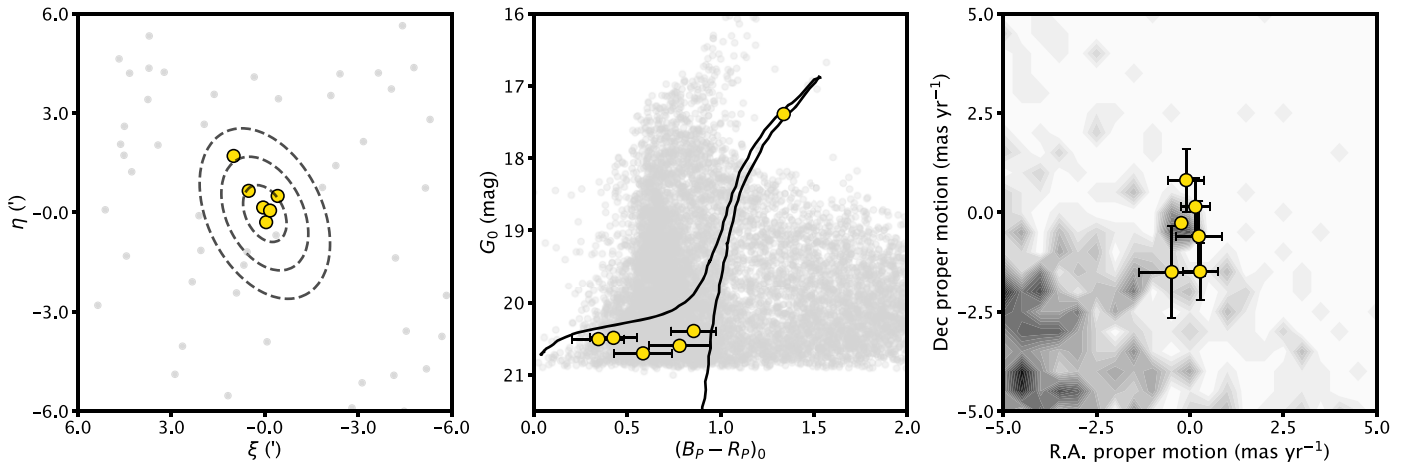


Figure 5. Yellow sources are those selected as high-confidence (probability $> 90\%$) members by our maximum-likelihood membership selection algorithm. Gray sources/shading are all five-parameter Gaia detections in a 2° circle around Boötes V. Left: sky positions of stars in a $12' \times 12'$ region about Boötes V, projected onto the tangent plane centered at R.A., decl. of $(14^{\text{h}}15^{\text{m}}38^{\text{s}}.6, +32^\circ 54' 42'')$. Center: CMD with a 13 Gyr, $[\text{Fe}/\text{H}] = -2.2$ isochrone overlaid. Right: proper motions of members overlaid on Milky Way foreground stars.

($\lambda\lambda 8498.02, 8542.09, 8662.14 \text{ \AA}$) and the absolute magnitude of the star M_V (see Equation A.1 from Starkenburg et al. 2010). The EW is measured using the SPLIT routine in IRAF (Tody 1986, 1993) fitting with multiple line profiles. The median and the standard deviation have been adopted as final values for the EW and its uncertainty, respectively. M_V is derived by converting the Gaia DR3 magnitudes to the Johnson-Cousin filter following the relation from Riello et al. (2021) and adopting a heliocentric distance of 100 ± 20 kpc. We perform a Monte Carlo analysis with 10^6 randomizations on the heliocentric distance, the EW, and the de-reddened magnitudes assuming Gaussian distributions for all parameters. The final $[\text{Fe}/\text{H}]$ and its uncertainty are the median and the standard deviation of the randomizations, respectively. The star is measured to be a very metal-poor star, with $[\text{Fe}/\text{H}] = -2.85 \pm 0.10$ dex.

To calculate the radial velocity, we create a synthetic spectrum using the *synth* option in MOOG¹² (Snedden 1973) with the list of spectral lines generated by LINEMAKE¹³ (Placco et al. 2021). We adopted a model atmosphere from the MARCS1 models (Gustafsson et al. 2008; Plez 2012). The synthetic spectrum has been created at the same resolution of the GMOS spectrograph with the stellar parameters T_{eff} , $\log g$, and $[\text{Fe}/\text{H}]$, where each parameter is derived with the following methods. The effective temperature is derived using the calibration from Mucciarelli et al. (2021), which takes as input the knowledge on the nature of the star (i.e., dwarf or giant), the metallicity, and the de-reddened Gaia EDR3 photometry. Then, the surface gravity is inferred adopting the Stefan-Boltzmann equation. This requires the distance, the de-reddened G magnitude, the bolometric corrections on the flux (Andrae et al. 2018), an estimate on the effective temperature, and the stellar mass ($0.5\text{--}0.8 M_\odot$). A Monte Carlo randomization has been performed to infer the T_{eff} , $\log g$, and their uncertainties. These methods have proved to yield robust stellar parameters compatible with high-resolution spectroscopic values in the very metal-poor regime (e.g., KIELTY et al. 2021; SESTITO et al. 2023; WALLER et al. 2023). We derive $T_{\text{eff}} = 4481 \pm 77$ K and $\log g = 0.87 \pm 0.11$, and incorporate

these parameters into the synthetic spectrum. Then, we added a Poissonian noise to match the observations. The radial velocity is measured by cross-correlating the combined observed spectrum with the downgraded synthetic spectrum using the FXCOR routine in IRAF, and is found to be $5.1 \pm 13.4 \text{ km s}^{-1}$. In the absence of any other stars in Boötes V with measured radial velocities, we adopt this radial velocity as representative of the systemic velocity of the candidate dwarf.

4.3. Orbital Analysis

We now use a simple dynamical model to examine the orbit of Boötes V, with the aim of understanding its orbital history and interaction with the Milky Way. We approximate Boötes V as a point-mass in a Milky Way potential, implemented with the PYTHON-wrapped package GALA (Price-Whelan 2017). The Milky Way potential used for this analysis is identical to that which is described in Jensen et al. (2021), so we direct the reader to that work, and references therein, for full details.

We perform 1000 realizations of the point-mass orbit, where the initial conditions (i.e., input parameters $\{\alpha_{J2000}, \delta_{J2000}, d, \mu_\alpha \cos \delta, \mu_\delta, v_r\}$) for each realization are drawn from normal distributions with means and standard deviations defined by the values and associated error bars presented in Table 2.

Each point-mass is integrated both forward and backward in time by 1 Gyr in time steps of 10^{-3} Gyr. For each orbit, the pericenter (closest approach to Milky Way), apocenter (furthest point from Milky Way), Z max (maximum height above the disk), time between pericenters (orbital time), time since last pericenter, and orbital eccentricity are recorded and presented in 1D distributions in Figure 6.

5. Classification and Conclusions

In this paper we have presented the discovery of the Boötes V satellite of the Milky Way in UNIONS. We detected it using a matched-filter method on the combined CFIS-*r* and Pan-STARRS-*i* photometric catalog, from which we estimated the distance, luminosity, and structural parameters of the system. Examination of the Gaia DR3 data allows us to confirm this as a real system, identify its brightest members in the Gaia data, and estimate its proper motion. GMOS-N observations also

¹² <https://www.as.utexas.edu/~chris/moog.html>

¹³ <https://github.com/vmplacco/linemake>

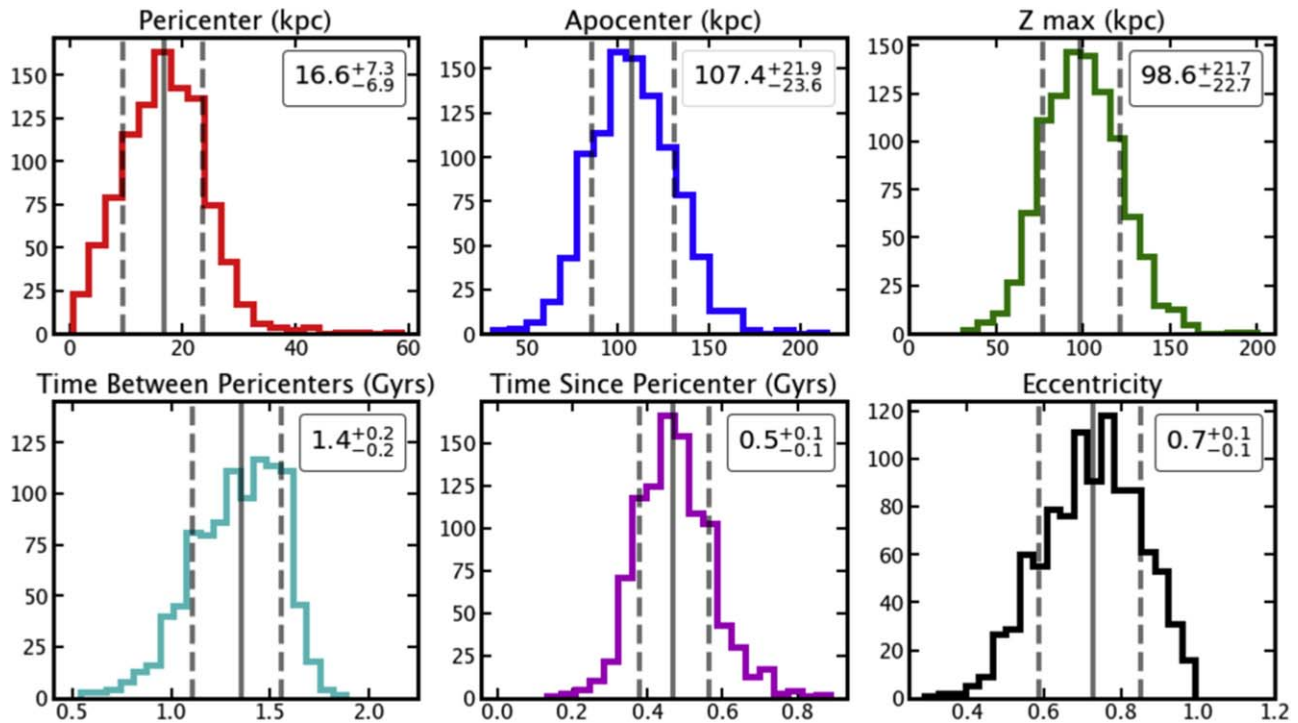


Figure 6. Resulting 1D distributions of key parameters from orbital MCMC analysis. It is estimated to take ~ 1.4 Gyr for Boötes V to travel between pericenters, and it has been ~ 0.5 Gyr since last pericenter.

allow us to provide a first estimate of its spectroscopic metallicity and its radial velocity, which in turn allow us to characterize the orbit of the system.

Based on the results of the orbital estimation, Boötes V is approaching the apocenter of its orbit, having been at pericenter ~ 0.5 Gyr ago. Interestingly, the pericenter of the orbit is $16.6^{+7.3}_{-6.9}$ kpc from the center of the Milky Way. With an orbital period of 1.4 Gyr, Boötes V may have had time to complete several orbits. Several such close passes with the inner part of the Milky Way potential may mean that tidal forces have affected this satellite, though there does not appear to be significant visual evidence in support of tidal disruption. Additionally, the orbit is highly eccentric, and the motion of the satellite is primarily occurring perpendicular to the disk.

We note, however, that the measure of a single radial velocity is a poor proxy for the systemic radial velocity of the satellite, as both dwarf galaxies and globular clusters are measured to have velocity dispersions on a scale of a few to tens of kilometers per second. We also note that the observed star for which we obtained spectroscopy is a visual double, with a companion that does not have fully measured astrometric parameters in Gaia DR3. However, the double is separated on the sky by $1''.72$, which, at a distance of 100 kpc, corresponds to a minimum physical separation of 0.83 pc. It is very unlikely that these two stars are bound, and if they are, a negligible portion of the radial velocity on the measured star would be due to binary orbital motion. Regardless, the radial velocity of this single, bright RGB star is still our best available tool for providing an initial estimate of the orbit for Boötes V.

Boötes V is faint ($M_V = -4.6 \pm 0.4$ mag), small ($r_h = 26.9^{+7.5}_{-3.4}$ pc), and distant ($d = 100 \pm 20$ kpc). A question remains as to whether this system is a dwarf galaxy or a globular cluster. Figure 7 illustrates the absolute V -band magnitude (M_V) versus half-light radius (r_h) plane, a commonly used metric for sorting dwarf galaxies and globular clusters.

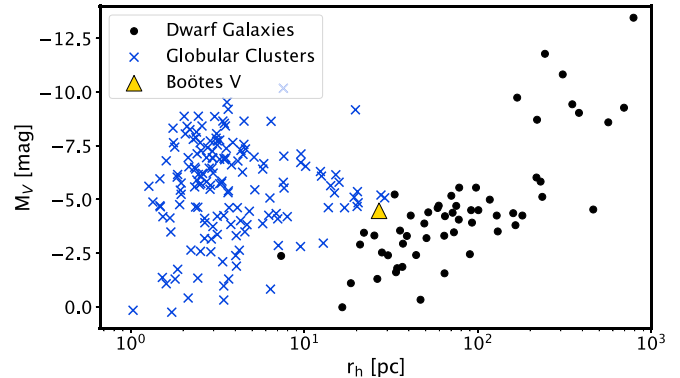


Figure 7. Absolute V -band magnitude (M_V) vs. half-light radius (r_h) plane showing both the dwarf galaxy (black markers) and globular cluster (blue “X” marks) populations. We show both candidate and spectroscopically confirmed dwarf galaxies within 300 kpc of the Milky Way. Boötes V is shown as a yellow triangle.

Here, we use only dwarf galaxies within 300 kpc of the Milky Way. The data and separation are taken from the updated data set of McConnachie (2012).¹⁴ For the globular clusters, we used data from Baumgardt & Vasiliev (2021).¹⁵ Boötes V resides in a region of this plane that has largely contained satellites whose classification has been contested. However, it is worth noting that, in terms of scale radius (r_h), Boötes V would be the third-largest globular cluster while only being the seventh-smallest dwarf. Additionally, at a heliocentric distance of 100 kpc, Boötes V would also be the fourth-most-distant globular cluster, but at a distance typical of dwarfs.

The metallicity of this system is very notable. The GMOS-N spectrum was measured to be very metal-poor, with an

¹⁴ <https://www.cadc-ccda.hia-ihp.nrc-cnrc.gc.ca/en/community/nearby/>

¹⁵ <https://people.smp.uq.edu.au/HolgerBaumgardt/globular/parameter.html>

$[\text{Fe}/\text{H}] = -2.85$ dex, indicating that Boötes V may be among the most metal-poor dwarf galaxies known. In terms of overall mean metallicities, Tucana II is the only dwarf with a mean metallicity more metal-poor than this, at -2.90 dex (Chiti et al. 2018). Four additional dwarf galaxies have $\langle [\text{Fe}/\text{H}] \rangle < -2.7$ (Boötes II, Draco II, Horologium I, and Segue 1; Frebel et al. 2014; Koposov et al. 2015b; Ji et al. 2016; Longeard et al. 2018; although the classification of Draco II is unclear at this time). Each of these five very metal-poor dwarfs contains individual stars that are measured to have $[\text{Fe}/\text{H}] \lesssim -3$ dex. While this single metallicity measurement certainly suggests Boötes V must be quite metal-poor, we do not yet know how representative this star is of the overall mean metallicity of the system, and more spectroscopic observations are needed.

Globular clusters do not appear to extend to such low mean metallicities as dwarf galaxies. Indeed, if Boötes V were a globular cluster, we would expect this single measurement to be more representative of the whole system, and it would be nearly 0.5 dex more metal-poor than the most extreme, *intact* globular cluster (Harris 1996, 2010 edition). However, it is worth noting that two remarkably metal-poor stellar streams have been discovered whose progenitors are thought to be ancient globular clusters, the Phoenix stellar stream (Wan et al. 2020), and the C-19 stellar stream (Martin et al. 2022), which have $[\text{Fe}/\text{H}] \simeq -2.70$ dex and $[\text{Fe}/\text{H}] \simeq -3.38$ dex, respectively.

The rather large caveat throughout this entire discussion is that we only have a metallicity measurement for a single star. However, it does immediately make Boötes V an interesting object of future spectroscopic studies, as results from the observations of several more stars will be two-fold: measurements of its stellar velocity dispersion will provide a direct estimation of the mass (and by extension, the dark matter content), and measurements of the metallicity dispersion have more recently been used as a proxy for mass, insofar as systems with a large metallicity dispersion likely need to reside, or have resided, in a massive dark matter halo (e.g., Willman & Strader 2012). Both measurements will likely provide clarity relating to the classification of this newly discovered system. While it is not inconceivable that this system could be a globular cluster, we consider the balance of evidence to currently suggest that Boötes V is more likely a member of the ever-growing class of UFDs.

Boötes V is the first Milky Way satellite to be discovered in the UNIONS data set, which, when complete, will provide coverage of approximately 5000 square degrees of the northern extragalactic sky at a depth comparable to the first year of the Legacy Survey of Space and Time by the Vera C. Rubin observatory. The discovery of a single new candidate dwarf galaxy is, in some sense, another drop in the bucket, as the list of known Local Group galaxies continues to grow quickly. Even though each new object is worthy of study in its own right, there is a more comprehensive goal underlying all of this work. The true power of broad searches for new dwarf galaxies is that they build toward amassing a statistically significant population of faint stellar systems whose chemical, dynamical, and structural properties will test theories of dark matter and of galaxy formation on the smallest scales.

Acknowledgments

We acknowledge and respect the $\text{l}\acute{\text{o}}\text{k}^{\text{w}}\acute{\text{o}}\eta\text{j}\acute{\text{o}}\text{n}$ peoples on whose traditional territory the University of Victoria stands and

the Songhees, Esquimalt and $\text{W}\acute{\text{S}}\acute{\text{A}}\text{N}\acute{\text{E}}\acute{\text{C}}$ peoples whose historical relationships with the land continue to this day.

It was a pleasure to coordinate the submission of this paper with an independent discovery paper led by William Cerny and the DELVE team, and we thank William, Alex Drlica-Wagner, and the whole DELVE team for the very positive, collaborative interactions that we had with them.

We thank the reviewer, whose comments and feedback helped improve the clarity and readability of this manuscript.

This work is based on data obtained as part of the Canada-France Imaging Survey, a CFHT large program of the National Research Council of Canada and the French Centre National de la Recherche Scientifique. Based on observations obtained with MegaPrime/MegaCam, a joint project of CFHT and CEA Saclay, at the Canada-France-Hawaii Telescope (CFHT), which is operated by the National Research Council (NRC) of Canada, the Institut National des Science de l'Univers (INSU) of the Centre National de la Recherche Scientifique (CNRS) of France, and the University of Hawaii. This research used the facilities of the Canadian Astronomy Data Centre operated by the National Research Council of Canada with the support of the Canadian Space Agency. This research is based in part on data collected at Subaru Telescope, which is operated by the National Astronomical Observatory of Japan. We are honored and grateful for the opportunity of observing the universe from Maunakea, which has significant cultural, historical, and natural significance in Hawaii. Pan-STARRS is a project of the Institute for Astronomy of the University of Hawaii, and is supported by the NASA SSO Near Earth Observation Program under grants 80NSSC18K0971, NNX14AM74G, NNX12AR65G, NNX13AQ47G, NNX08AR22G, and YORPD20_2-0014 and by the State of Hawaii.

We thank the staff of Gemini Observatory North for their support in the acquisition of some of these data. We are also grateful to the director of Gemini for granting us Directors Discretionary time to complete this study. These data are based on observations obtained at the international Gemini Observatory, a program of NSF's NOIRLab, which is managed by the Association of Universities for Research in Astronomy (AURA) under a cooperative agreement with the National Science Foundation on behalf of the Gemini Observatory partnership: the National Science Foundation (United States), National Research Council (Canada), Agencia Nacional de Investigación y Desarrollo (Chile), Ministerio de Ciencia, Tecnología e Innovación (Argentina), Ministério da Ciência, Tecnologia, Inovações e Comunicações (Brazil), and Korea Astronomy and Space Science Institute (Republic of Korea).

This work has made use of data from the European Space Agency (ESA) mission Gaia (<https://www.cosmos.esa.int/gaia>), processed by the Gaia Data Processing and Analysis Consortium (DPAC, <https://www.cosmos.esa.int/web/gaia/dpac/consortium>). Funding for the DPAC has been provided by national institutions, in particular the institutions participating in the Gaia Multilateral Agreement.





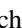







Guoshoujing Telescope (the Large Sky Area Multi-Object Fiber Spectroscopic Telescope LAMOST) is a National Major Scientific Project built by the Chinese Academy of Sciences. Funding for the project has been provided by the National Development and Reform Commission. LAMOST is operated and managed by the National Astronomical Observatories, Chinese Academy of Sciences.

A.W.M. acknowledges support from the NSERC Discovery Grant program. N.F.M. gratefully acknowledges support from the French National Research Agency (ANR) funded project “Pristine” (ANR-18-CE31-0017) along with funding from the European Research Council (ERC) under the European Unions Horizon 2020 research and innovation program (grant agreement No. 834148). F.S. thanks the Dr. Margaret “Marmie” Perkins Hess postdoctoral fellowship for funding his work at the University of Victoria.

Facilities: CFHT, PS1, Gemini:Gillett, Gaia.

Software: *astropy* (Astropy Collaboration et al. 2013, 2018, 2022), *emcee* (Foreman-Mackey et al. 2013), *numpy* (Harris et al. 2020), *scipy* (Virtanen et al. 2020).

ORCID iDs

Simon E. T. Smith  <https://orcid.org/0000-0002-6946-8280>
 Joel Roediger  <https://orcid.org/0000-0002-0363-4266>
 Federico Sestito  <https://orcid.org/0000-0002-3182-3574>
 Christian R. Hayes  <https://orcid.org/0000-0003-2969-2445>
 Alan W. McConnachie  <https://orcid.org/0000-0003-4666-6564>
 Stephen Gwyn  <https://orcid.org/0000-0001-8221-8406>
 Eugene Magnier  <https://orcid.org/0000-0002-7965-2815>
 Ken Chambers  <https://orcid.org/0000-0001-6965-7789>
 Francois Hammer  <https://orcid.org/0000-0002-2165-5044>
 Mike J. Hudson  <https://orcid.org/0000-0002-1437-3786>
 Nicolas Martin  <https://orcid.org/0000-0002-1349-202X>
 Julio Navarro  <https://orcid.org/0000-0003-3862-5076>

References

- Abazajian, K. N., Adelman-McCarthy, J. K., Agüeros, M. A., et al. 2009, *ApJS*, 182, 543
- Abbott, T. M. C., Abdalla, F. B., Allam, S., et al. 2018, *ApJS*, 239, 18
- Andrae, R., Fouesneau, M., Creevey, O., et al. 2018, *A&A*, 616, A8
- Astropy Collaboration, Price-Whelan, A. M., Lim, P. L., et al. 2022, *ApJ*, 935, 167
- Astropy Collaboration, Price-Whelan, A. M., Sipőcz, B. M., et al. 2018, *AJ*, 156, 123
- Astropy Collaboration, Robitaille, T. P., Tollerud, E. J., et al. 2013, *A&A*, 558, A33
- Baumgardt, H., & Vasiliev, E. 2021, *MNRAS*, 505, 5957
- Bechtol, K., Drlica-Wagner, A., Balbinot, E., et al. 2015, *ApJ*, 807, 50
- Belokurov, V., Walker, M. G., Evans, N. W., et al. 2008, *ApJL*, 686, L83
- Belokurov, V., Zucker, D. B., Evans, N. W., et al. 2006, *ApJL*, 647, L111
- Belokurov, V., Zucker, D. B., Evans, N. W., et al. 2007, *ApJ*, 654, 897
- Bovill, M. S., & Ricotti, M. 2009, *ApJ*, 693, 1859
- Bressan, A., Marigo, P., Girardi, L., et al. 2012, *MNRAS*, 427, 127
- Bullock, J. S., & Boylan-Kolchin, M. 2017, *ARA&A*, 55, 343
- Bullock, J. S., Kravtsov, A. V., & Weinberg, D. H. 2000, *ApJ*, 539, 517
- Cerny, W., Martínez-Vázquez, C. E., Drlica-Wagner, A., et al. 2023a, *ApJ*, 953, 1
- Cerny, W., Pace, A. B., Drlica-Wagner, A., et al. 2021a, *ApJ*, 910, 18
- Cerny, W., Pace, A. B., Drlica-Wagner, A., et al. 2021b, *ApJL*, 920, L44
- Cerny, W., Simon, J. D., Li, T. S., et al. 2023b, *ApJ*, 942, 111
- Chambers, K. C., Magnier, E. A., Metcalfe, N., et al. 2016, arXiv:1612.05560
- Chiti, A., Frebel, A., Ji, A. P., et al. 2018, *ApJ*, 857, 74
- Collins, M. L. M., Charles, E. J. E., Martínez-Delgado, D., et al. 2022, *MNRAS*, 515, L72
- Darragh-Ford, E., Nadler, E. O., McLaughlin, S., & Wechsler, R. H. 2021, *ApJ*, 915, 48
- Deason, A. J., Belokurov, V., & Evans, N. W. 2011, *MNRAS*, 416, 2903
- Dey, A., Schlegel, D. J., Lang, D., et al. 2019, *AJ*, 157, 168
- Drlica-Wagner, A., Bechtol, K., Rykoff, E. S., et al. 2015, *ApJ*, 813, 109
- Drlica-Wagner, A., Carlin, J. L., Nidever, D. L., et al. 2021, *ApJS*, 256, 2
- Drlica-Wagner, A., Ferguson, P. S., Adamów, M., et al. 2022, *ApJS*, 261, 38
- Flaugher, B., Diehl, H. T., Honscheid, K., et al. 2015, *AJ*, 150, 150
- Foreman-Mackey, D., Hogg, D. W., Lang, D., & Goodman, J. 2013, *PASP*, 125, 306
- Frebel, A., Simon, J. D., & Kirby, E. N. 2014, *ApJ*, 786, 74
- Freedman, W. L., Madore, B. F., Hoyt, T., et al. 2020, *ApJ*, 891, 57
- Gaia Collaboration 2022, *yCat*, I/358
- Gaia Collaboration, Brown, A. G. A., Vallenari, A., et al. 2021, *A&A*, 649, A1
- Gaia Collaboration, Prusti, T., de Bruijne, J. H. J., et al. 2016, *A&A*, 595, A1
- Gustafsson, B., Edvardsson, B., Eriksson, K., et al. 2008, *A&A*, 486, 951
- Harris, C. R., Millman, K. J., van der Walt, S. J., et al. 2020, *Natur*, 585, 357
- Harris, W. E. 1996, *AJ*, 112, 1487
- Jensen, J., Thomas, G., McConnachie, A. W., et al. 2021, *MNRAS*, 507, 1923
- Ji, A. P., Frebel, A., Simon, J. D., & Geha, M. 2016, *ApJ*, 817, 41
- Kielty, C. L., Venn, K. A., Sestito, F., et al. 2021, *MNRAS*, 506, 1438
- Koposov, S. E., Belokurov, V., Torrealba, G., & Evans, N. W. 2015a, *ApJ*, 805, 130
- Koposov, S. E., Casey, A. R., Belokurov, V., et al. 2015b, *ApJ*, 811, 62
- Kroupa, P. 2001, *MNRAS*, 322, 231
- Laevens, B. P. M., Martin, N. F., Bernard, E. J., et al. 2015a, *ApJ*, 813, 44
- Laevens, B. P. M., Martin, N. F., Ibata, R. A., et al. 2015b, *ApJL*, 802, L18
- Lee, M. G., Freedman, W. L., & Madore, B. F. 1993, *ApJ*, 417, 553
- Lindegren, L., Klioner, S. A., Hernández, J., et al. 2021, *A&A*, 649, A2
- Longard, N., Martin, N., Starkenburg, E., et al. 2018, *MNRAS*, 480, 2609
- Lovell, M. R., Eke, V., Frenk, C. S., et al. 2012, *MNRAS*, 420, 2318
- Martin, N. F., de Jong, J. T. A., & Rix, H.-W. 2008, *ApJ*, 684, 1075
- Martin, N. F., Ibata, R. A., Lewis, G. F., et al. 2016, *ApJ*, 833, 167
- Martin, N. F., Ibata, R. A., McConnachie, A. W., et al. 2013, *ApJ*, 776, 80
- Martin, N. F., Venn, K. A., Aguado, D. S., et al. 2022, *Natur*, 601, 45
- Martínez-Delgado, D., Karim, N., Charles, E. J. E., et al. 2022, *MNRAS*, 509, 16
- Mau, S., Cerny, W., Pace, A. B., et al. 2020, *ApJ*, 890, 136
- McConnachie, A. W. 2012, *AJ*, 144, 4
- McConnachie, A. W., Huxor, A., Martin, N. F., et al. 2008, *ApJ*, 688, 1009
- McConnachie, A. W., Irwin, M. J., Ibata, R. A., et al. 2009, *Natur*, 461, 66
- McConnachie, A. W., & Venn, K. A. 2020a, *AJ*, 160, 124
- McConnachie, A. W., & Venn, K. A. 2020b, *RNAAS*, 4, 229
- Mucciarelli, A., Bellazzini, M., & Massari, D. 2021, *A&A*, 653, A90
- Piatti, A. E., Hwang, N., Cole, A. A., Angelo, M. S., & Emptage, B. 2018, *MNRAS*, 481, 49
- Placco, V. M., Sneden, C., Roederer, I. U., et al. 2021, *RNAAS*, 5, 92
- Plez, B. 2012, Turbospectrum: Code for Spectral Synthesis, Astrophysics Source Code Library, ascl:1205.004
- Price-Whelan, A. M. 2017, *JOSS*, 2, 388
- Richardson, J. C., Irwin, M. J., McConnachie, A. W., et al. 2011, *ApJ*, 732, 76
- Riello, M., De Angeli, F., Evans, D. W., et al. 2021, *A&A*, 649, A3
- Salaris, M., & Cassisi, S. 1997, *MNRAS*, 289, 406
- Sand, D. J., Mutlu-Pakdil, B., Jones, M. G., et al. 2022, *ApJL*, 935, L17
- Schlafly, E. F., & Finkbeiner, D. P. 2011, *ApJ*, 737, 103
- Schlegel, D. J., Finkbeiner, D. P., & Davis, M. 1998, *ApJ*, 500, 525
- Sesar, B., Hernitschek, N., Mitrović, S., et al. 2017, *AJ*, 153, 204
- Sestito, F., Venn, K. A., Arentsen, A., et al. 2023, *MNRAS*, 518, 4557
- Simon, J. D. 2019, *ARA&A*, 57, 375
- Sneden, C. A. 1973, PhD thesis, The Univ. Texas at Austin
- Starkenburg, E., Hill, V., Tolstoy, E., et al. 2010, *A&A*, 513, A34
- Tody, D. 1986, *Proc. SPIE*, 627, 733
- Tody, D. 1993, in ASP Conf. Ser. 52, Astronomical Data Analysis Software and Systems II, ed. R. J. Hanisch, R. J. V. Brissenden, & J. Barnes (San Francisco, CA: ASP), 173
- Torrealba, G., Belokurov, V., Koposov, S. E., et al. 2018, *MNRAS*, 475, 5085
- Torrealba, G., Belokurov, V., Koposov, S. E., et al. 2019, *MNRAS*, 488, 2743
- Torrealba, G., Koposov, S. E., Belokurov, V., & Irwin, M. 2016, *MNRAS*, 459, 2370
- Virtanen, P., Gommers, R., Oliphant, T. E., et al. 2020, *NatMe*, 17, 261
- Waller, F., Venn, K., Sestito, F., et al. 2023, *MNRAS*, 519, 1349
- Wan, Z., Lewis, G. F., Li, T. S., et al. 2020, *Natur*, 583, 768
- Wheeler, C., Oñorbe, J., Bullock, J. S., et al. 2015, *MNRAS*, 453, 1305
- Willman, B., Blanton, M. R., West, A. A., et al. 2005a, *AJ*, 129, 2692
- Willman, B., Dalcanton, J. J., Martínez-Delgado, D., et al. 2005b, *ApJL*, 626, L85
- Willman, B., & Strader, J. 2012, *AJ*, 144, 76
- Xiang, M., Ting, Y.-S., Rix, H.-W., et al. 2019, *ApJS*, 245, 34
- York, D. G., Adelman, J., Anderson, J. E. J., et al. 2000, *AJ*, 120, 1579